



Synthesis of uniform-sized bimetallic iron–nickel phosphide nanorods

Ki Youl Yoon^a, Youngjin Jang^a, Jongnam Park^a, Yosun Hwang^b, Bonil Koo^a,
Je-Geun Park^b, Taeghwan Hyeon^{a,*}

^a National Creative Research Initiative Center for Oxide Nanocrystalline Materials, School of Chemical and Biological Engineering, Seoul National University, Seoul 151-744, Republic of Korea

^b Department of Physics and Institute of Basic Science, Sungkyunkwan University, Suwon 440-746, Republic of Korea

ARTICLE INFO

Article history:

Received 23 February 2008

Received in revised form

23 April 2008

Accepted 3 May 2008

Available online 21 May 2008

Keywords:

Metal phosphides

Nanorods

Magnetic

ABSTRACT

We synthesized uniform-sized nanorods of iron–nickel phosphides from the thermal decomposition of metal–phosphine complexes. Uniform-sized $(\text{Fe}_x\text{Ni}_{1-x})_2\text{P}$ nanorods ($0 \leq x \leq 1$) of various compositions were synthesized by thermal decomposition of Ni–trioctylphosphine (TOP) complex and Fe–TOP complex. By measuring magnetic properties, we found that blocking temperature and coercive field depend on Ni content in the nanorods. Both parameters were more sensitive to doping compared with bulk samples.

© 2008 Elsevier Inc. All rights reserved.

1. Introduction

Nanocrystals exhibit distinct electronic, optical, magnetic, and chemical properties compared with their bulk counterparts [1]. There have been many reports on the synthesis of monodisperse nanocrystals having controlled sizes. One-dimensional (1-D) nanostructures including nanorods, nanowires, and nanotubes, have received tremendous attention because of their novel and intriguing properties and many technological applications. During the past decade, various 1-D nanostructured materials have been synthesized using different procedures [2]. For example, our research group reported the synthesis of various monodisperse nanocrystals of metals, metal oxides, and metal chalcogenides [3]. Chaudret and coworkers reported the synthesis of cobalt and nickel nanorods from thermal decomposition of organometallic complexes [4]. Puentes et al. [5] reported the synthesis of cobalt nanodisks via thermal decomposition of $\text{Co}_2(\text{CO})_8$ in hot solvent in the presence of surfactants. Metal phosphides exhibit many interesting electronic, catalytic, and magnetic properties, and recently various nanorods of transition metal phosphides have been synthesized [6]. Hexagonal iron phosphide and related materials have been intensively studied for their ferromagnetism, magneto-resistance and magnetocaloric effect [7]. Consequently, it would be very interesting to study the size and shape dependent characteristics of nanostructured metal phosphides.

Several methods have been reported for the synthesis of metal phosphides, including solvothermal reactions, decomposition of single-source precursors, organometallic approach, and thermal decomposition of metal complexes [8–15]. In particular, Brock et al. [9] reported the synthesis of various metal phosphide nanocrystals. They showed that phosphine surfactants could serve both as stabilizing ligands and as phosphorus source [9]. Brock categorized the synthesis of transition metal phosphides as unsupported and supported particles [9]. Recently, her research group synthesized MnP nanorods by hot-injection of $\text{Mn}_2(\text{CO})_{10}$ in hot solvent mixture of trioctylphosphine oxide and TOP and found no influence of shape anisotropy on the magnetic properties [10]. Liu and coworkers reported antiferromagnetic FeP nanorods and nanowires via the thermal decomposition of a precursor/surfactant mixture solution using a syringe pump [11]. Recently, Schaak and coworkers reported generalized synthesis of metal phosphide nanocrystals using TOP as phosphorus source [13]. Our group reported on the synthesis of uniformly sized nanorods of various metal phosphides from the thermal decomposition of continuously delivered metal–phosphine complexes using a syringe pump [14,15]. Bimetallic nanocrystals often exhibit enhanced properties compared with monometallic counterparts. Bimetallic magnetic nanocrystals such as FePt, CoPt, MnFe_2O_4 , and CoFe_2O_4 have been synthesized [16]. In this article, we report on the synthesis of bimetallic Fe–Ni phosphide nanorods from the thermal decomposition of the mixture of Fe–TOP and Ni–TOP complexes. We also characterized the magnetic properties of these bimetallic phosphide nanorods.

* Corresponding author. Fax: +82 2 886 8457.

E-mail address: thyeon@snu.ac.kr (T. Hyeon).

2. Experimental section

2.1. Chemicals

Hexane, ethanol, and acetone were distilled and degassed before use. Tri-*n*-octylphosphine (TOP, 90%), nickel acetylacetonate ($\text{Ni}(\text{acac})_2$, 97%), and iron pentacarbonyl ($\text{Fe}(\text{CO})_5$, 99.999%) were purchased from Aldrich Chemicals.

2.2. Synthesis of $(\text{Fe}_x\text{Ni}_{1-x})_2\text{P}$ nanorods

The synthetic procedure of bimetallic phosphides is similar to those for the synthesis of Fe_2P nanocrystals, which employs the thermal decomposition of metal–phosphine complexes. In case of $(\text{Fe}_{0.90}\text{Ni}_{0.10})_2\text{P}$, the Fe–TOP complex solution was prepared by adding 0.3 mL of $\text{Fe}(\text{CO})_5$ (2.28 mM) in 3 mL of TOP at 130 °C. The resulting reaction mixture was heated to 315 °C, and then 4 mL of Ni–TOP complex solution prepared by mixing 0.05 g of $\text{Ni}(\text{acac})_2$ and 4 mL of TOP was injected within 1 min at 315 °C. The solution was maintained at 315 °C for 2 h, producing iron–nickel phosphide nanorods with average dimensions of 4 nm × 16 nm (Fig. 1a). To synthesize $(\text{Fe}_{0.80}\text{Ni}_{0.20})_2\text{P}$, 4 mL of Ni–TOP complex solution, prepared by mixing 0.15 g of $\text{Ni}(\text{acac})_2$ and 4 mL of TOP, was injected continuously using a syringe pump for 1 h to the Fe–TOP complex solution at 315 °C. The solution was maintained at 315 °C for 2 h, yielding iron–nickel phosphide nanorods with average dimensions of 4 nm × 14 nm (Fig. 1b). For the synthesis of $(\text{Fe}_{0.75}\text{Ni}_{0.25})_2\text{P}$ nanorods, the Ni–TOP complex solution prepared from the reaction of 0.25 g of $\text{Ni}(\text{acac})_2$ and 4 mL of TOP was delivered continuously to the Fe–TOP solution using a syringe pump at 315 °C for 2 h, producing nanorods of average dimensions of 4 nm × 13 nm (Fig. 1c). After the injection, the resulting solution was maintained at 315 °C for 2 h, and then the reaction was stopped by cooling to ~60 °C under argon flow. The solution was then treated with 50 mL of ethanol and 50 mL of acetone to form a black brown precipitate and the $(\text{Fe}_x\text{Ni}_{1-x})_2\text{P}$ nanorod powder was obtained by centrifugation.

2.3. Characterization of materials

Metal phosphide nanorods were characterized by low- and high-resolution transmission electron microscopy (TEM), electron

diffraction, and X-ray diffraction (XRD). TEM images were collected on a JEOL JEM-2010 electron microscope operating at 200 kV. Samples for TEM analysis were prepared by putting a drop of organic solution containing the nanorods on the surface of a copper grid coated with an amorphous carbon film. XRD patterns were obtained using a Rigaku D/Max-3C diffractometer equipped with a rotation anode and a $\text{CuK}\alpha$ radiation source ($\lambda = 0.15418$ nm). The magnetic properties of the $(\text{Fe}_x\text{Ni}_{1-x})_2\text{P}$ nanorods were characterized using a commercial SQUID magnetometer, (MPMS-5XL, Quantum Design, USA) which measures magnetization from 2 to 380 K and up to 5 T. All our magnetization measurements were carried out after zero field cooling (ZFC) from room temperature. The KDS 100 syringe pump was employed for continuous and well-controlled release of metal–surfactant complex.

3. Results and discussion

The iron–nickel phosphide nanorods were synthesized by the solution–phase thermal decomposition of continuously delivered Ni–TOP complexes using a syringe pump in a hot surfactant solution containing Fe–TOP complexes [14,15]. Using a syringe pump assured the continuous and constant delivery of Ni–TOP complex into the Fe–TOP complex solution, and inducing thermal decomposition and 1-D growth of iron–nickel phosphide nanorods. When single or multiple injections of metal–phosphine complexes were performed without a syringe pump, polydisperse spherical nanoparticles and nanorods were produced. The overall growth process of the current nanorod formation is similar to the so-called seed-mediated growth mechanism of gold nanorods [17]. The main purpose of varying the injection rate of a syringe pump was to synthesize $(\text{Fe}_x\text{Ni}_{1-x})_2\text{P}$ nanorods with controlled compositions but with keeping similar aspect ratios.

Figs. 1a and d show 4 nm × 16 nm-sized $(\text{Fe}_{0.90}\text{Ni}_{0.10})_2\text{P}$ nanorods synthesized by the thermal decomposition of Fe–TOP and Ni–TOP complexes, which were prepared from the reaction of $\text{Fe}(\text{CO})_5$ and $\text{Ni}(\text{acac})_2$ with TOP. The length of $(\text{Fe}_{0.90}\text{Ni}_{0.10})_2\text{P}$ nanorods was inversely proportional to the injection rate of the Ni–TOP complex solution. This result is consistent with what we previously observed with Fe_2P nanorods synthesized from the thermal decomposition of syringe pump delivered Fe–TOP

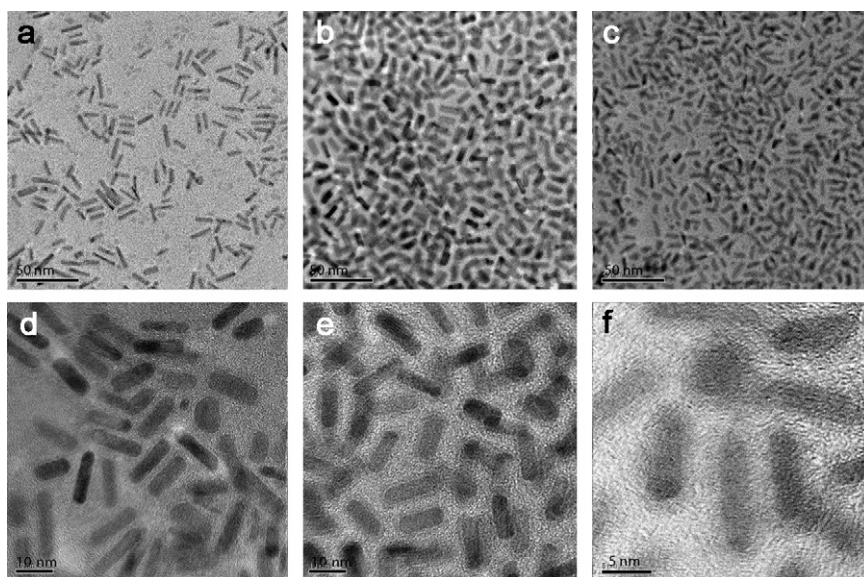


Fig. 1. TEM images of iron–nickel phosphide nanorods: (a, d) 4 nm × 16 nm-sized $(\text{Fe}_{0.90}\text{Ni}_{0.10})_2\text{P}$ nanorods; (b, e) 4 nm × 14 nm-sized $(\text{Fe}_{0.80}\text{Ni}_{0.20})_2\text{P}$ nanorods; (c, f) 4 nm × 13 nm-sized $(\text{Fe}_{0.75}\text{Ni}_{0.25})_2\text{P}$ nanorods.

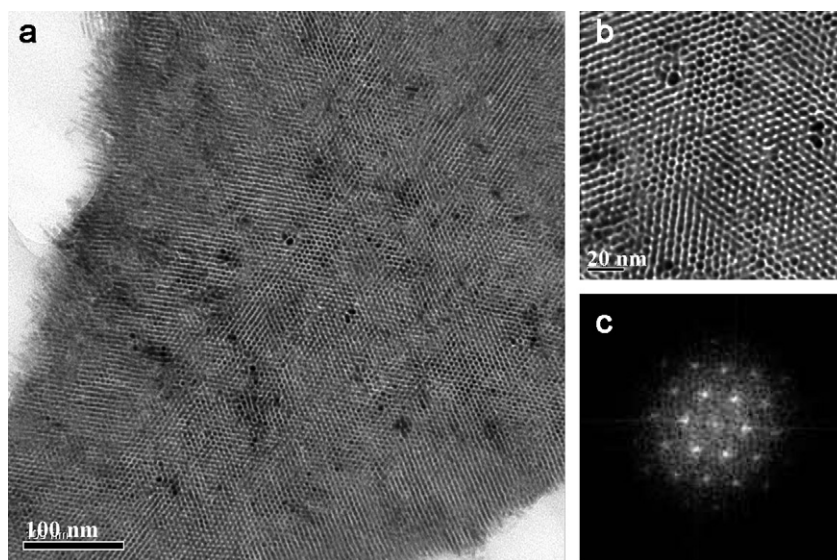


Fig. 2. (a) TEM image of long-range-ordered self-assembly of $(\text{Fe}_{0.90}\text{Ni}_{0.10})_2\text{P}$ nanorods. (b) High-magnification TEM image of the 3-D superlattice array of the $(\text{Fe}_{0.90}\text{Ni}_{0.10})_2\text{P}$ nanorods. (c) FFT image of $(\text{Fe}_{0.90}\text{Ni}_{0.10})_2\text{P}$ shows well-ordered hexagonal closed-packed structure.

complex [14]. In the case of $(\text{Fe}_{0.80}\text{Ni}_{0.20})_2\text{P}$, the Ni-TOP solution was added to the Fe-TOP solution at a injection rate of 4 mL/h via syringe pump, and the color of the reaction mixture turned to dark brown after ~ 10 min, indicating that nucleation occurred by the thermal decomposition of the Ni-TOP complex. When the reaction was completed, $(\text{Fe}_{0.80}\text{Ni}_{0.20})_2\text{P}$ nanorods of dimension $4\text{ nm} \times 14\text{ nm}$ were generated. For the synthesis of $(\text{Fe}_{0.75}\text{Ni}_{0.25})_2\text{P}$ nanorods, longer injection time was required to reach the same length and aspect ratio of $(\text{Fe}_{0.90}\text{Ni}_{0.10})_2\text{P}$ nanorods and $(\text{Fe}_{0.80}\text{Ni}_{0.20})_2\text{P}$ nanorods, demonstrating that the growth step is important for $(\text{Fe}_x\text{Ni}_{1-x})_2\text{P}$ nanorod length control, and the length of nanorods increases by decreasing the injection rate. These results demonstrate that the use of a syringe pump is critical for the formation of $(\text{Fe}_x\text{Ni}_{1-x})_2\text{P}$ nanorods, not spherical nanoparticles.

The formation of $(\text{Fe}_x\text{Ni}_{1-x})_2\text{P}$ nanorods along the $\langle 002 \rangle$ direction seems to be caused by the binding of TOP surfactants on lattice planes perpendicular to (002) plane and the intrinsic anisotropy of hexagonal close packed (hcp) crystal structure, as we previously reported in the synthesis of Fe_2P nanorods [14]. After the initial formation of spherical nanoparticles, growth subsequently occurs on these nanospheres along preferential direction, because strongly binding TOP seems to preferentially bind to the crystal growth face. To understand the importance of the TOP surfactant for the synthesis of the nanorods, we systematically decreased the relative amount of TOP, with all other experimental parameters unchanged. When the amount of TOP in the mixed solution was less than 2 mL, spherical nanoparticles were predominantly produced. When more than 5 mL of TOP was used in the synthesis, not only the thickness of nanorods decreased, but also the length of nanorods increased. The results indicate that a sufficient amount of TOP is required for the preferential growth along $\langle 002 \rangle$ direction by the effective stabilization of crystal faces perpendicular to (002) .

Fig. 2 shows the TEM image of long-range-ordered self-assembly of nanorods. In order to obtain the self-assembled structure, the solution was washed several times alternatively with 50 mL acetone and with 50 mL ethanol. The black brown precipitate of $(\text{Fe}_x\text{Ni}_{1-x})_2\text{P}$ nanorods was obtained by centrifugation. An extensive three-dimensional (3-D) hcp superlattice was formed along the $\langle 002 \rangle$ direction by slowly evaporating on a TEM grid (Fig. 2a). The high-magnification TEM image of the 3-D

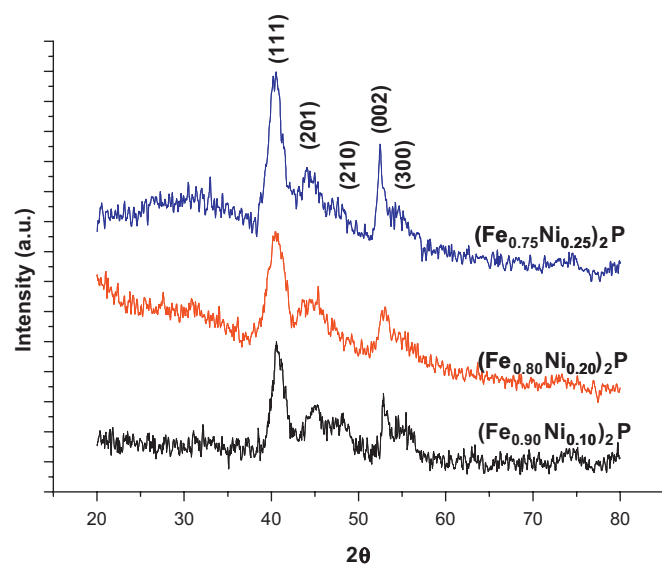


Fig. 3. X-ray diffraction patterns for $(\text{Fe}_x\text{Ni}_{1-x})_2\text{P}$ nanorods with $x = 0.75, 0.80,$ and 0.90 .

superlattice array of the $(\text{Fe}_{0.90}\text{Ni}_{0.10})_2\text{P}$ nanorods (Fig. 2b) and fast Fourier transform (FFT) image of $(\text{Fe}_{0.90}\text{Ni}_{0.10})_2\text{P}$ (Fig. 2c) confirm well-ordered hexagonal closed packed structure. A very similar result involving 3-D superlattice formation was observed in the case of the cobalt nanorods [4a] and the Fe_2P nanorods [14].

All of diffraction peaks in the XRD pattern can be indexed by the hexagonal Fe_2P structure and no extra reflection was observed, as shown in Fig. 3. In many 1-D nanocrystals grown along $\langle 001 \rangle$ direction, 001 lines are very sharp whereas $hk0$ reflections are broad. The (002) reflection in the XRD pattern was sharp, indicating the growth of the nanorods along the c -axis.

Fig. 4 shows the temperature dependence of the magnetization. As shown in the inset, magnetization increases upon cooling for both ZFC and field cooling (FC) curves before showing a maximum at which temperature the ZFC and FC data deviates from each other. These blocking temperatures (T_B) are found to be very sensitive to the Ni content as shown in Fig. 4. For example, T_B

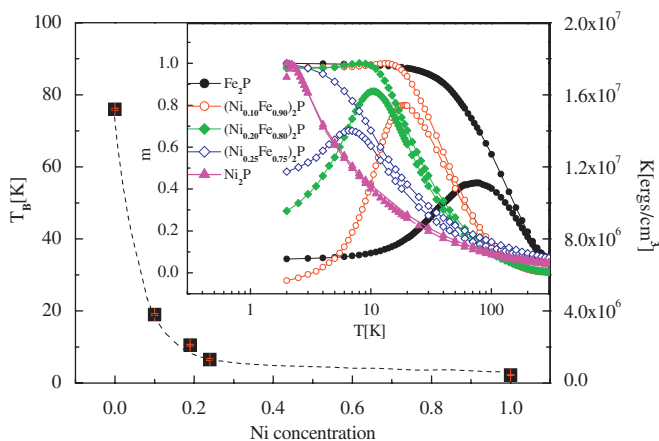


Fig. 4. Plot of Ni concentration dependence of blocking temperature (T_B). T_B was determined from the magnetization data given in the inset. The magnetization curves in the inset were normalized for comparison. We estimated the magnetic anisotropy energy (K) using the following relationship, $K = 25k_B T_B / V$, where V is the volume of an individual nanoparticle.

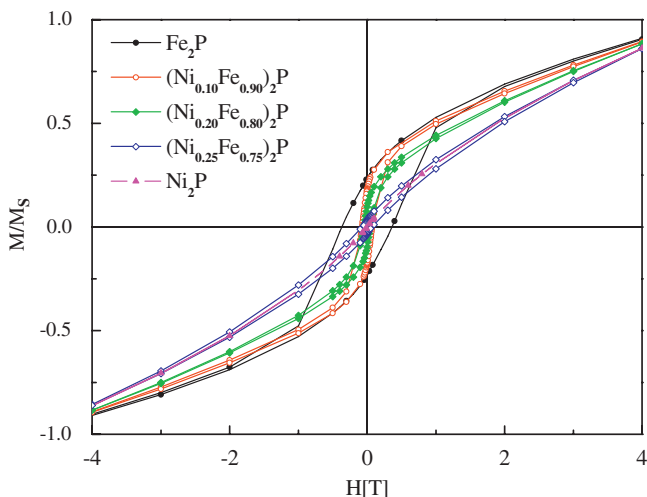


Fig. 5. Field dependence of the magnetization measured at 2 K by varying Ni content. The hysteresis loop becomes narrower with increasing Ni concentration, which is consistent with the doping dependence of T_B shown in Fig. 4.

is 76 K for pure Fe_2P and drops to 27 K for $(\text{Fe}_{0.90}\text{Ni}_{0.10})_2\text{P}$. With more than 20% Ni concentration, the blocking temperature decreases gradually and the pure Ni_2P nanorods has a blocking temperature of 2.2 K. We note that the magnetic anisotropy energy (K) estimated from the blocking temperature is 1.49×10^7 erg/cm³, slightly smaller than that of bulk sample, $K = 2.3 \times 10^7$ erg/cm³ [18]. The field dependence of the magnetization in Fig. 5 shows that the hysteresis loop becomes smaller with increasing Ni concentration. This doping dependence of the coercive field is consistent with the fact that the blocking temperature gets significantly reduced upon Ni doping. There are few points worth noting in the magnetic properties of the nanorods. First, we note that the doping dependence of the blocking temperature seems to be markedly stronger than that found in bulk samples [19]. According to the bulk magnetic studies, the magnetic properties are found to be linear in Ni concentration up to 50% of Ni doping. As the magnetic anisotropy energy K is proportional to the square of the saturated magnetization, therefore we would expect that the blocking temperature should be proportional to the square of the Ni concentration, at least in a low doping range. However, our

results show that the blocking temperature drops faster than that expected for the bulk measurements. Secondly, our Ni_2P nanoparticles show blocking behavior unlike bulk Ni_2P , which is nonmagnetic [20]. This difference between nanoparticles and bulk samples can be ascribed to so-called surface uncompensated spin [21].

4. Conclusions

In summary, we synthesized Fe–Ni bimetallic phosphide nanorods via thermal decomposition of metal–surfactant precursors. The current synthetic procedure is highly reproducible, and the compositions can be readily tuned by varying the ratios of the Fe and Ni precursors. Magnetic studies revealed that unlike bulk Ni_2P , the blocking temperature is significantly reduced upon Ni doping [20], which can be explained by uncompensated surface spin [21].

Acknowledgment

T.H. would like to thank the National Creative Research Initiative Program of the Korean Ministry of Science and Technology for the financial support. Works at Sungkyunkwan University were supported by the Proton Accelerator User Program (no. M102KSO10001-02K1901-01810) of Proton Engineering R&D Project and the Center for Strongly Correlated Materials Research.

References

- [1] (a) Y. Xia, P. Yang, *Adv. Mater.* 15 (2003) 351–352; (b) Y. Cui, C.M. Lieber, *Science* 291 (2001) 851–853; (c) T.T. Hanrath, B.A. Korgel, *J. Am. Chem. Soc.* 124 (2001) 1424; (d) G. Schmid, *Nanoparticles: from Theory to Application*, Wiley-VCH, Weinheim, 2004; (e) K.J. Klabunde, *Nanoscale Materials in Chemistry*, Wiley-Interscience, New York, 2001; (f) J.H. Fendler, *Nanoparticles and Nanostructured Films*, Wiley-VCH, Weinheim, 1998; (g) A.P. Alivisatos, *Science* 271 (1996) 933–937; (h) C. Pacholski, A. Kornowski, H. Weller, *Angew. Chem. Int. Ed.* 41 (2002) 1188–1191; (i) T. Hyeon, *Chem. Commun.* (2003) 927–934; (j) H.B. Na, J.H. Lee, K. An, Y.I. Park, M. Park, I.S. Lee, D.-H. Nam, S.T. Kim, S.-H. Kim, S.-W. Kim, K.-H. Lim, K.-S. Kim, S.-O. Kim, T. Hyeon, *Angew. Chem. Int. Ed.* 46 (2007) 5397–5401.
- [2] Y. Xia, P. Yang, Y. Sun, Y. Wu, B. Mayers, B. Gates, Y. Yin, F. Kim, H. Yan, *Adv. Mater.* 15 (2003) 353–389 and its references.
- [3] (a) S.-J. Park, S. Kim, S. Lee, Z.G. Khim, K. Char, T. Hyeon, *J. Am. Chem. Soc.* 122 (2000) 8581–8582; (b) K. An, N. Lee, J. Park, S.C. Kim, Y. Hwang, J.-G. Park, J.-Y. Kim, J.-H. Park, M.J. Han, J. Yu, T. Hyeon, *J. Am. Chem. Soc.* 128 (2006) 9753–9760; (c) J. Joo, S.G. Kwon, T. Yu, M. Cho, J. Lee, J. Yoon, T. Hyeon, *J. Phys. Chem. B* 109 (2005) 15297–15302; (d) B. Koo, J. Park, Y. Kim, S.-H. Choi, Y.-E. Sung, T. Hyeon, *J. Phys. Chem. B* 110 (2006) 24318–24323; (e) J. Joo, S.G. Kwon, J.H. Yu, T. Hyeon, *Adv. Mater.* 17 (2005) 1873–1877; (f) J.H. Yu, J. Joo, H.M. Park, S.-I. Baik, Y.W. Kim, S.C. Kim, T. Hyeon, *J. Am. Chem. Soc.* 127 (2005) 5662–5670.
- [4] (a) F. Dumestre, B. Chaudret, C. Amiens, M. Respaud, P. Fejes, P. Renaud, P. Zurcher, *Angew. Chem. Int. Ed.* 42 (2003) 5213–5216; (b) F. Dumestre, B. Chaudret, C. Amiens, M.-C. Fromen, M.-J. Casanove, M. Respaud, P. Zurcher, *Angew. Chem. Int. Ed.* 41 (2002) 4286–4289.
- [5] (a) V.F. Puntes, K.M. Krishnan, A.P. Alivisatos, *Science* 291 (2001) 2115–2117; (b) V.F. Puntes, D. Zanchet, C.K. Erdonmez, A.P. Alivisatos, *J. Am. Chem. Soc.* 124 (2002) 12874–12880.
- [6] (a) B. Aronsson, T. Lundström, S. Rundqvist, *Borides, Silicides and Phosphides*, Wiley, New York, 1965; (b) N.N. Greenwood, A. Earnshaw, *Chemistry of the Elements*, Pergamon Press, New York, 1994; (c) C. Stinner, R. Prins, Th. Weber, *J. Catal.* 202 (2001) 187–194; (d) C.M. Lukehart, S.B. Milne, S.R. Stock, *Chem. Mater.* 10 (1988) 903–908.

- [7] (a) F. Luo, H.-L. Su, W. Song, Z.-M. Wang, Z.-G. Yan, C.-H. Yan, *J. Mater. Chem.* 14 (2004) 111–115;
(b) O. Tegus, E. Brück, K.H.J. Buschow, F.R. de Boer, *Nature* 415 (2002) 150–152.
- [8] (a) S.C. Perera, G. Tsoi, L.E. Wenger, S.L. Brock, *J. Am. Chem. Soc.* 125 (2003) 13960–13961;
(b) K.L. Stamm, J.C. Garno, G.-y. Liu, S.L. Brock, *J. Am. Chem. Soc.* 125 (2003) 4038–4039;
(c) S.C. Perera, P. Fodor, G. Tsoi, L.E. Wenger, S.L. Brock, *Chem. Mater.* 15 (2003) 4034–4038;
(d) K.A. Gregg, S.C. Perera, G. Lawes, S. Shinozaki, S.L. Brock, *Chem. Mater.* 18 (2006) 879–886.
- [9] S.L. Brock, C. Susanthri, S.C. Perera, K.L. Stamm, *Chem. Eur. J.* 10 (2004) 3364–3371.
- [10] K. Senevirathne, A.W. Burns, M.E. Bussell, S.L. Brock, *Adv. Funct. Mater.* 17 (2007) 3933–3939.
- [11] C. Qian, F. Kim, L. Ma, F. Tsui, P. Yang, J. Liu, *J. Am. Chem. Soc.* 126 (2004) 1195–1198.
- [12] (a) J.-H. Chen, M.-F. Tai, K.-M. Chi, *J. Mater. Chem.* 14 (2004) 296–298;
(b) Y. Li, M.A. Malik, P. O'Brien, *J. Am. Chem. Soc.* 127 (2005) 16020–16021;
(c) R.-K. Chiang, R.-T. Chiang, *Inorg. Chem.* 46 (2007) 369–371;
(d) A.T. Kelly, I. Rusakova, T. Ould-Ely, C. Hofmann, A. Luttge, K.H. Whitmire, *Nano Letters* 7 (2007) 2920–2925;
(e) Y. Xie, H.L. Su, X.F. Zian, X.M. Liu, Y.T. Qian, *J. Solid State Chem.* 149 (2000) 88–91;
(f) G. Yunle, G. Fan, Y.T. Qian, Z. Huangui, Y. Ziping, *Mater. Res. Bull.* 37 (2002) 1101–1105.
- [13] (a) A.E. Henkes, Y. Vasquez, R.E. Schaak, *J. Am. Chem. Soc.* 129 (2007) 1896–1897;
(b) A.E. Henkes, R.E. Schaak, *Chem. Mater.* 19 (2007) 4234–4242.
- [14] J. Park, B. Koo, Y. Hwang, C. Bae, K. An, J.-G. Park, H.M. Park, T. Hyeon, *Angew. Chem. Int. Ed.* 43 (2004) 2282–2285.
- [15] J. Park, B. Koo, K.Y. Yoon, Y. Hwang, J.-G. Park, T. Hyeon, *J. Am. Chem. Soc.* 127 (2005) 8433–8440.
- [16] (a) H. Gu, P.-L. Ho, K.W.T. Tsang, L. Wang, B. Xu, *J. Am. Chem. Soc.* 125 (2003) 15702–15703;
(b) F.J. Himpfel, J.E. Ortega, G.J. Mankey, R.F. Willis, *Adv. Phys.* 47 (1998) 511–597;
(c) I.J. Jeon, D.W. Kang, E.D. Kim, D.H. Kim, S.B. Choe, S.C. Shin, *Appl. Surf. Sci.* 197–198 (2002) 639–643;
(d) C.T. Black, C.B. Murray, R.L. Sandstrom, S. Sun, *Science* 290 (2000) 1131–1134;
(e) J.J. Schneider, *Adv. Mater.* 13 (2001) 529–533;
(f) K.A. Easom, K.J. Klabunde, C.M. Sorensen, *Polyhedron* 13 (1994) 1197–1223;
(g) J. Rockenberger, E.C. Scher, A.P. Alivisatos, *J. Am. Chem. Soc.* 121 (1999) 11595–11596;
(h) K.V.P.M. Shafi, A. Gedanken, *Chem. Mater.* 10 (1998) 3445–3450;
(i) Q. Guo, X. Teng, S. Rahman, H. Yang, *J. Am. Chem. Soc.* 125 (2003) 630–631.
- [17] (a) C.J. Murphy, N.R. Jana, *Adv. Mater.* 14 (2002) 80–82;
(b) A. Gole, C.J. Murphy, *Chem. Mater.* 16 (2004) 3633–3640;
(c) J.X. Gao, C.M. Bender, C.J. Murphy, *Langmuir* 19 (2003) 9065–9070;
(d) B. Nikoobakht, M.A. El-Sayed, *Chem. Mater.* 15 (2003) 1957–1962;
(e) C.J. Johnson, E. Dujardin, S.A. Davis, C.J. Murphy, S. Mann, *J. Mater. Chem.* 12 (2002) 1765–1770;
(f) N.R. Jana, L. Gearheart, C.J. Murphy, *Adv. Mater.* 13 (2001) 1389–1393;
(g) N.R. Jana, L. Gearheart, C.J. Murphy, *Chem. Mater.* 13 (2001) 2313–2322.
- [18] H. Fujii, T.H. Okabe, T. Kamigaichi, T. Okamoto, *J. Phys. Soc. Jpn.* 43 (1977) 41–46.
- [19] R. Zach, J. Tobola, B. Sredniawa, S. Kaprzyk, C. Sasado, M. Bacmann, D. Fruchart, *J. Alloys Compds.* 383 (2004) 322–327.
- [20] S. Ohta, H. Onmayashiki, *Physica B* 253 (1998) 193–202.
- [21] R.H. Kodama, S.A. Makhlof, A.E. Berkowitz, *Phys. Rev. Lett.* 79 (1997) 1393–1396.